Theor Chem Acc (2011) 130:227–236
DOI 10.1007/s00214-011-0963-3

REGULAR ARTICLE

Theoretical studies on a new pattern of laser-driven systems: towards elucidation of direct photo-injection in dye-sensitized solar cells

Kenji Mishima · Hiroshi Segawa · Koichi Yamashita

Received: 26 February 2011 / Accepted: 13 May 2011 / Published online: 3 June 2011

Abstract In this paper, we theoretically and numerically investigate a new type of analytically solvable laser-driven systems inspired by electron-injection dynamics in dye-sensitized solar cells. The simple analytical expressions are found to be useful for understanding the difference between dye excitation and direct photo-injection occurring between dye molecule and semiconductor nanoparticles. More importantly, we propose a method for discriminating experimentally dye excitation and direct photo-injection using time-dependent fluorescence. We have found that dye excitation shows no significant quantum beat, whereas the direct photo-injection shows a significant quantum beat.

Keywords Laser-driven systems · Direct photo-injection · Dye-sensitized solar cells

1 Introduction

Physical and chemical phenomena triggered by external perturbations (e.g., laser pulses, magnetic fields, etc.) have long attracted much attention, especially since the advent of lasers [1–4]. In particular, the factors that enable the use of lasers for many application purposes are their coherence, high monochromaticity, and ability to reach extremely high powers. Applications of lasers include laser spectroscopy [5], interferometry, laser cooling, and control of physical and chemical reactions [6, 7], to name a few. Given that such a wide range of applications for lasers have been discovered so far, one can expect lasers to be of use for many purposes that have yet to be considered.

Close examination of the quantum systems that are irradiated by lasers reveals that a variety of patterns have been studied. First, the two-state model, where one transition is triggered by the incident oscillatory field, has been studied extensively [1], and analytical expressions can easily be derived. The second model studied is the three-state system [8–11]. In two symmetric cases, the time-dependent Schrödinger equation including external fields can analytically be solved and simplified [12]. Less symmetric three-level systems have been analytically derived using of Clausen's special function [13, 14]. The energy-level configuration of the so-called Λ structure has also been studied extensively [15], and the most general *N*-level system has been analyzed [16–23]. In [17], the time-dependent Schrödinger equation,

$$i\hbar \frac{\mathrm{d}}{\mathrm{d}t} C_n(t) = \sum_m W_{nm} C_m(t), \tag{1}$$

where the Hamiltonian W is tridiagonal and stepwise excitation of nondegenerate levels took place, was treated. Recently, stimulated Raman adiabatic passage (STIRAP), which is a method of using partially overlapping pulses (from pump to Stokes lasers) to produce complete population transfer between two quantum states, has received much attention [24].

Dedicated to Professor Shigeru Nagase on the occasion of his 65th birthday and published as part of the Nagase Festschrift Issue.

K. Mishima · H. Segawa
Research Center for Advanced Science and Technology, The University of Tokyo, 4-6-1, Komaba, Meguro-ku, Tokyo 153-8904, Japan

K. Yamashita (✉)
Department of Chemical System Engineering, Graduate School of Engineering, The University of Tokyo, Tokyo 113-8656, Japan
e-mail: yamasita@chemsys.t.u-tokyo.ac.jp

Meanwhile, dye-sensitized solar cells have been extensively developed experimentally in the quest for efficient conversion of solar energy to electricity [25, 26]. It is argued that electron injection from dye to semiconductor takes place via dye excitation or direct photo-injection (interfacial charge-transfer transition) [27]. In almost all of the dye molecules, dye excitation from the HOMO to the LUMO via sunlight and then electron injection from the LUMO to the semiconductor conduction band is the most common scenario. However, a direct photo-injection scheme that does not involve the LUMO of the adsorbate has been proposed for catechol attached to TiO_2 nanoparticles using quantum chemical INDO/S-CI calculations [28], periodic density functional theory (DFT) [29], and molecular orbital theory and density functional theory [30], as well as experimentally [31–34]. In addition, TCNE, TCNQ, and TCNAQ molecules attached to TiO_2 nanoparticles are also predicted to be candidates for direct photo-injection experimentally [35]. This is because the energy gap between the HOMO of the molecule and the conduction band minimum of TiO_2, ΔE, approximately agrees with the onset energy of the broad-band absorption spectrum. In contrast, in [36], ab initio DFT molecular dynamics simulations were performed for electron transfer in catechol/TiO_2—anatase nanostructures based on the above common scenario. This implies that there is no agreement if the electron injection for the above systems occurs via dye excitation or a direct photo-injection mechanism. However, no experimental evidence or theoretical proposal to discriminate dye excitation and direct photo-injection has been reported so far. Therefore, it is very important to find a method to discriminate between these two electron-injection mechanisms. We show below that time-dependent fluorescence is a versatile tool for this purpose.

The present paper is organized as follows. In Sect. 2, we model electron-injection dynamics under laser-pulse irradiation using a simple model. At the expense of exactness, we show that the analytical derivation and calculations based on such analytical expressions are quite useful for elucidation of the more accurate calculations that follow in the next section. In addition, we extend the theory proposed by May et al. [37] to take into account direct photo-injection. In Sect. 3, we show and discuss numerical results and clarify the usefulness of laser-pulse irradiation and time-dependent fluorescence for discrimination between dye excitation and direct photo-injection. Section 4 is devoted to concluding remarks.

2 Theory

Figure 1 shows two mechanisms for electron transfer from dye molecule to semiconductor detected experimentally or predicted theoretically: dye excitation and direct photo-injection (interfacial charge-transfer transition). This figure reminds us of the simplified photo-excitation scheme shown in Fig. 2a. In the figure, the ground state is photo-excited by laser pulses to the excited state, which is then coupled to many states (considered as continuum states) via the coupling constant V. This type of laser-driven system has not yet been investigated. Moreover, as a first step and a prototype for the purpose of elucidating of the difference between dye excitation and direct photo-injection, this model system is worthy of detailed study, as shown below.

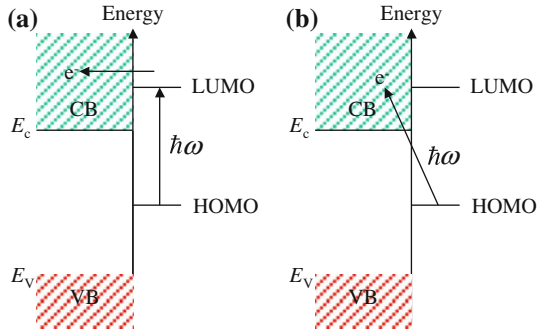

Fig. 1 Comparison between dye excitation (**a**) and direct photo-injection (interfacial charge-transfer transition) (**b**). CB and VB stand for conduction band and valence band of the TiO_2 nanoparticles, respectively. The quantities, E_c and E_v, are the energies of the conduction band minimum and valence band maximum, respectively

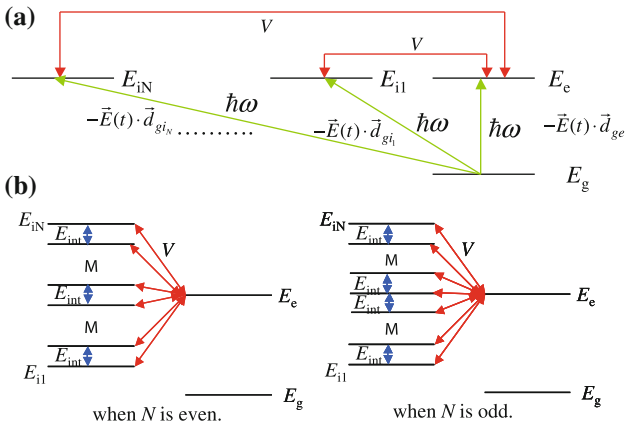

Fig. 2 **a** Energy-level diagram that mimics electron injection from the HOMO (direct photo-injection or interfacial charge-transfer transition) or LUMO (dye excitation) of the attached dye molecule to the interior of the TiO_2 nanoparticle. **b** Energy-level diagram for exact numerical calculations using the Schrödinger equation (2). The energy gap between the adjacent continuum states is denoted by E_{int}

$$i\hbar\frac{\mathrm{d}}{\mathrm{d}t}\begin{bmatrix} c_g(t) \\ c_e(t) \\ c_{i_1}(t) \\ c_{i_2}(t) \\ \vdots \\ c_{i_N}(t) \end{bmatrix} = \begin{bmatrix} E_g & -\vec{E}(t)\cdot\vec{d}_{ge} & -\vec{E}(t)\cdot\vec{d}_{gi_1} & -\vec{E}(t)\cdot\vec{d}_{gi_2} & \cdots & -\vec{E}(t)\cdot\vec{d}_{gi_N} \\ -\vec{E}(t)\cdot\vec{d}_{eg} & E_e & V & V & \cdots & V \\ -\vec{E}(t)\cdot\vec{d}_{i_1g} & V & E_{i_1} & 0 & \cdots & 0 \\ -\vec{E}(t)\cdot\vec{d}_{i_2g} & V & 0 & E_{i_2} & 0 & \vdots \\ \vdots & \vdots & \vdots & 0 & \vdots & 0 \\ -\vec{E}(t)\cdot\vec{d}_{i_Ng} & V & 0 & \cdots & 0 & E_{i_N} \end{bmatrix} \begin{bmatrix} c_g(t) \\ c_e(t) \\ c_{i_1}(t) \\ c_{i_2}(t) \\ \vdots \\ c_{i_N}(t) \end{bmatrix}, \tag{2}$$

The Schrödinger equation for this system is given by where $\vec{d}_{ge}$ and $\vec{d}_{eg}$ are the transition dipole moments between the ground state g and excited state e, and $\vec{d}_{gi_j}$ and $\vec{d}_{i_jg}$ are those between state g and the continuum state i_j. The parameter N represents the number of ionized (continuum) states of the conduction band of the semiconductor taken into account in the calculations. The symbols E_m and $c_m(t)$ are the eigenenergy and coefficient of the wave function of state m, respectively. For simplicity, we assume that the incident laser field is a square laser pulse so that $\vec{E}(t)$ is written as

$$\vec{E}(t) = \vec{E}_0\cos(\omega t) \tag{3}$$

Note that the off-diagonal terms $-\vec{E}(t)\cdot\vec{d}_{gi_1}$, $-\vec{E}(t)\cdot\vec{d}_{gi_2},\ldots,-\vec{E}(t)\cdot\vec{d}_{gi_N}$, $-\vec{E}(t)\cdot\vec{d}_{i_1g}$, $-\vec{E}(t)\cdot\vec{d}_{i_2g},\ldots$, and $-\vec{E}(t)\cdot\vec{d}_{i_Ng}$, which represent the direct photo-injection to the continuum from the ground state g, have been ignored so far.

When $\vec{d}_{ge}=\vec{d}_{eg}$, $\vec{d}_{gi_1}=\vec{d}_{gi_2}=\cdots=\vec{d}_{gi_N}=\vec{d}_{i_1g}=\vec{d}_{i_2g}=\cdots=\vec{d}_{i_Ng}=\vec{d}_{gi}$, and $E_e-E_g=E_{i_1}-E_g=E_{i_2}-E_g=\cdots=E_{i_N}-E_g=\hbar\omega$ (the laser pulse is resonant with all the states, e and i), Eq. 2 can be solved analytically by invoking the rotating-wave approximation. This assumption might be very crude, but from the uncertainty principle $\Delta E\cdot\Delta t\sim\hbar/2$ and the shortness of the laser pulse used in the calculations in the next section (100 fs), the assumption is almost valid because numerous states can be simultaneously coherently pumped under such a condition. Then, the solutions are given by

$$c_n(t) = d_n(t)\exp(-iE_nt/\hbar)\quad (n=g,e,i_1,i_2,\ldots,i_N), \tag{4}$$

where

$$d_g(t) = d_g^{(1)}\exp(s_1t)+d_g^{(2)}\exp(s_2t)+d_g^{(3)}\exp(s_3t), \tag{5}$$

$$d_e(t) = d_e^{(1)}\exp(s_1t)+d_e^{(2)}\exp(s_2t)+d_e^{(3)}\exp(s_3t), \tag{6}$$

$$d_i(t) = d_i^{(1)}\exp(s_1t)+d_i^{(2)}\exp(s_2t)+d_i^{(3)}\exp(s_3t), \tag{7}$$

$$\begin{aligned} &s^3+\left\{\frac{\left(\vec{E}_0\cdot\vec{d}_{ge}\right)^2}{4\hbar^2}+N\left(\frac{\left(\vec{E}_0\cdot\vec{d}_{gi}\right)^2}{4\hbar^2}+\frac{V^2}{\hbar^2}\right)\right\}s \\ &\quad-\frac{iNV}{2\hbar^3}\left(\vec{E}_0\cdot\vec{d}_{ge}\right)\left(\vec{E}_0\cdot\vec{d}_{gi}\right) \\ &\quad=(s-s_1)(s-s_2)(s-s_3)=0 \end{aligned} \tag{8}$$

$$\begin{aligned} d_g^{(1)} &= \frac{s_1^2+NV^2/\hbar^2}{(s_1-s_2)(s_1-s_3)},\quad d_g^{(2)}=\frac{s_2^2+NV^2/\hbar^2}{(s_2-s_1)(s_2-s_3)}, \\ d_g^{(3)} &= \frac{s_3^2+NV^2/\hbar^2}{(s_3-s_1)(s_3-s_2)}, \\ d_e^{(1)} &= \frac{NV\vec{E}_0\cdot\vec{d}_{gi}/2\hbar^2+is_1\vec{E}_0\cdot\vec{d}_{ge}/2\hbar}{(s_1-s_2)(s_1-s_3)}, \\ d_e^{(2)} &= \frac{NV\vec{E}_0\cdot\vec{d}_{gi}/2\hbar^2+is_2\vec{E}_0\cdot\vec{d}_{ge}/2\hbar}{(s_2-s_1)(s_2-s_3)}, \\ d_e^{(3)} &= \frac{NV\vec{E}_0\cdot\vec{d}_{gi}/2\hbar^2+is_3\vec{E}_0\cdot\vec{d}_{ge}/2\hbar}{(s_3-s_1)(s_3-s_2)}, \\ d_i^{(1)} &= \frac{V\vec{E}_0\cdot\vec{d}_{ge}/2\hbar^2+is_1\vec{E}_0\cdot\vec{d}_{gi}/2\hbar}{(s_1-s_2)(s_1-s_3)}, \\ d_i^{(2)} &= \frac{V\vec{E}_0\cdot\vec{d}_{ge}/2\hbar^2+is_2\vec{E}_0\cdot\vec{d}_{gi}/2\hbar}{(s_2-s_1)(s_2-s_3)}, \\ d_i^{(3)} &= \frac{V\vec{E}_0\cdot\vec{d}_{ge}/2\hbar^2+is_3\vec{E}_0\cdot\vec{d}_{gi}/2\hbar}{(s_3-s_1)(s_3-s_2)}, \end{aligned} \tag{9}$$

for $0\le t\le t_{\mathrm{off}}$.

On the other hand,

$$d_g(t) = d_g(t_{\mathrm{off}}), \tag{10}$$

$$\begin{aligned} d_e(t) &= d_4\exp\left\{i\sqrt{N}V(t-t_{\mathrm{off}})/\hbar\right\} \\ &\quad+d_5\exp\left\{-i\sqrt{N}V(t-t_{\mathrm{off}})/\hbar\right\}, \end{aligned} \tag{11}$$

$$d_i(t) = -\frac{d_4}{\sqrt{N}}\exp\left\{i\sqrt{N}V(t-t_{\text{off}})/\hbar\right\} + \frac{d_5}{\sqrt{N}}\exp\left\{-i\sqrt{N}V(t-t_{\text{off}})/\hbar\right\}, \quad (12)$$

$$d_4 = \frac{d_e(t_{\text{off}}) - \sqrt{N}d_i(t_{\text{off}})}{2}, \quad d_5 = \frac{d_e(t_{\text{off}}) + \sqrt{N}d_i(t_{\text{off}})}{2}, \quad (13)$$

for $t_{\text{off}} \le t \le t_{\text{final}}$.

Here, t_{off} is the time when the incident laser pulse is switched off, and t_{final} is the final time of the time evolution. Even without any calculations, some conclusions can be drawn from the above analytical expressions. First, from Eqs. 4–7, it can be concluded that when the laser pulse is on, the populations of each state show both oscillatory and decaying behaviors depending on the roots of Eq. 8, which are usually complex. Second, from Eqs. 10–13, it can also be concluded that when the laser pulse is off, the population of state g does not change with time and that the pure oscillatory population time evolutions of the states e and i become more frequent with increasing N.

The relaxation of the injected electron to the conduction band minimum owing to coupling to vibrations was successfully taken into account by May et al. [37]. Extending their theory to take into account the direct photo-injection, the Hamiltonian of the system is expressed as

$$H(t) = H_{\text{mol-sem}} + H_{\text{field}}(t), \quad (14)$$

where

$$H_{\text{mol-sem}} = \sum_{a=g,e,\vec{k}} \{E_a + H_a(q)\}|\varphi_a\rangle\langle\varphi_a| + \sum_{\vec{k}} \left(V_{\vec{k}e}|\varphi_{\vec{k}}\rangle\langle\varphi_e| + h.c.\right), \quad (15)$$

$$H_{\text{field}}(t) = -\vec{E}(t)\cdot\hat{\vec{\mu}}, \quad (16)$$

$$\hat{\vec{\mu}} = \vec{d}_{eg}|\varphi_e\rangle\langle\varphi_g| + \sum_{\vec{k}} \vec{d}_{\vec{k}g}|\varphi_{\vec{k}}\rangle\langle\varphi_g| + h.c. \quad (17)$$

Here, $|\varphi_g\rangle$, $|\varphi_e\rangle$, and $|\varphi_{\vec{k}}\rangle$ represent the electronic wave functions for HOMO, LUMO, and ionized state with the wave vector $\vec{k}$. E_g, E_e, and $E_{\vec{k}}$ are the energy minima, and $H_g(q)$, $H_e(q)$, and $H_{\vec{k}}(q)$ represent the vibrational Hamiltonians of the electronic states. HOMO, LUMO, and ionized state with the wave vector $\vec{k}$, respectively. $V_{\vec{k}e}$ is the coupling of the band states to LUMO. The abbreviation, h. c., denotes the Hermitian conjugate. From the above definitions, it turns out that the Schrödinger equation to be solved is given by

$$\frac{dc_{gL}(t)}{dt} = -i\left(E_g/\hbar + \omega_L\right)c_{gL}(t) + \frac{i}{\hbar}\vec{E}(t)\cdot\vec{d}_{ge}\sum_M \langle\chi_{gL}|\chi_{eM}\rangle c_{eM}(t) + \frac{i}{\hbar}\vec{E}(t)\cdot\vec{d}_{gi}\sum_p\sum_M \langle\chi_{gL}|\chi_{\text{ion}M}\rangle\langle\mathcal{N}u_p\rangle c_M^{(p)}(t) \quad (18)$$

$$\frac{dc_{eL}(t)}{dt} = -i(E_e/\hbar + \omega_L)c_{eL}(t) + \frac{i}{\hbar}\vec{E}(t)\cdot\vec{d}_{eg}\sum_M \langle\chi_{eL}\mid\chi_{gM}\rangle c_{gM}(t) - \frac{i}{\hbar}\sum_p\sum_M \langle\chi_{eL}\mid\chi_{\text{ion}M}\rangle\langle\mathcal{N}Vu_p\rangle c_M^{(p)}(t) \quad (19)$$

$$\frac{dc_L^{(r)}(t)}{dt} = -i(E_c/\hbar + \omega_L)c_L^{(r)}(t) + \frac{i}{\hbar}\vec{E}(t)\cdot\vec{d}_{ig}\sum_M \langle\chi_{\text{ion}L}\mid\chi_{gM}\rangle\langle\mathcal{N}u_r\rangle c_{gM}(t) - i\sum_p \langle\omega u_r u_p\rangle c_L^{(p)}(t) - \frac{i}{\hbar}\sum_M \langle u_r V\rangle \times \langle\chi_{\text{ion}L}\mid\chi_{eM}\rangle c_{eM}(t) \quad (20)$$

In these equations, we have taken the direct photo-injection by incident light into consideration by including the terms $\vec{E}(t)\cdot\vec{d}_{gi}$ and $\vec{E}(t)\cdot\vec{d}_{ig}$. Here, E_c is the lowest energy of the ionized states. The integers L and M count the vibrational quantum numbers. The wave functions $|\chi_{gM}\rangle$, $|\chi_{eM}\rangle$, and $|\chi_{\text{ion}M}\rangle$ denote the vibrational eigenfunctions of the HOMO, LUMO, and ionized states of the adsorbed molecule having the vibrational quantum number M, respectively. The operator, $\aleph$, is the density of states of the conduction band of the semiconductor: $\aleph(\omega) = \sum_k \delta(\omega - \omega_k)$ [37]. The coefficients, $c_{gM}(t)$, $c_{eM}(t)$, and $c_M^{(r)}(t)$, represent wave function coefficients for the HOMO and LUMO having the vibrational quantum number M, and the ionized state having both the vibrational quantum number M and the integer r that appears in the function $u_r(\omega)$, which is expressed by Legendre polynomials, respectively. The function $u_r(\omega)$ concretely reads

$$u_r(\omega) = \sqrt{\frac{2r+1}{\omega_{\max}}}P_r[x(\omega)], \quad (21)$$

where

$$x(\omega) = \frac{2\omega}{\omega_{\max}} - 1, \quad (22)$$

and $P_r(x)$ is the Legendre polynomial,

$$P_r(x) = \frac{1}{2^r r!}\left(\frac{d}{dx}\right)^r (x^2-1)^r. \quad (23)$$

Here, $\omega_{\max}$ characterizes the frequency interval from the lower to the upper conduction band edge. The vibrational eigenenergy, $\hbar\omega_M$, is given by

$$\hbar\omega_M = \hbar(M + 1/2)\omega_{\text{vib}}, \tag{24}$$

because we assume harmonic potentials for the HOMO, LUMO, and ionized states. In all the calculations shown in the next section, we assume $\hbar\omega_{\text{vib}} = 0.1$ eV.

In the approximation of a uniform density of states $\bar{\mathcal{N}}$ and a frequency-independent transfer coupling $\bar{V}$ (wide-band approximation), we have

$$\langle u_r V\rangle = \delta_{r,0}\bar{V}\sqrt{\omega_{\max}}, \tag{25}$$

$$\langle \omega u_r u_p\rangle = \frac{\omega_{\max}}{2}\left(\delta_{r,p+1}\sqrt{\frac{(p+1)^2}{4(p+1)^2-1}} + \delta_{r,p} + \delta_{r,p-1}\sqrt{\frac{p^2}{4p^2-1}}\right), \tag{26}$$

$$\langle \mathcal{N} V u_p\rangle = \delta_{p,0}\bar{\mathcal{N}}\bar{V}\sqrt{\omega_{\max}}, \tag{27}$$

$$\langle \mathcal{N} u_p\rangle = \delta_{p,0}\bar{\mathcal{N}}\sqrt{\omega_{\max}}. \tag{28}$$

Here, the bracket $\langle\cdots\rangle$ denotes frequency integration according to the following relationship,

$$\langle F\rangle \equiv \int_0^{\omega_{\max}} d\omega F(\omega). \tag{29}$$

The time-dependent fluorescence, $I(t)$, is expressed as in [38]:

$$I(t) = K\sum_{f,n}\left|\vec{d}_{nf}\right|^2\rho_{nn} + K\sum_{f,n\neq n'}\vec{d}_{n'f}\cdot\vec{d}_{fn}\rho_{nn'}, \tag{30}$$

where K is a constant, f is the HOMO because the final state f is HOMO in the fluorescence process, and

$$\rho_{nn'}(t) = c_n(t)c^*_{n'}(t), \tag{31}$$

which is the density matrix. In the harmonic-potential approximation, the Franck–Condon factor for the displaced harmonic potentials is given by

$$\langle\chi_{aL}\mid\chi_{bM}\rangle = \exp(-S/2)\sum_{j=0}^{M}\sum_{k=0}^{L}\delta_{L-k,M-j}S^{(j+k)/2} \times\frac{M!(-1)^k}{j!(M-j)!k!}\sqrt{\frac{L!}{M!}}. \tag{32}$$

In this equation, S is the so-called Huang-Rhys factor and is defined by

$$S = \omega_{vib}/2\hbar(\Delta Q)^2, \tag{33}$$

where ΔQ is the displacement in the normal mode coordinate of the potential energy surfaces.

3 Numerical results and discussion

In this section, we show the numerical results using the analytical expressions and more exact differential equations derived in the previous section and also propose a method of discriminating direct photo-injection and dye excitation in dye-sensitized solar cells. In all of the calculations presented below, t_{off} was set to be 100 fs. In addition, the wavelength of the incident laser pulse was 420 nm ($\hbar\omega = 2.952$ eV), assuming that the dye molecule is catechol and V was set to be 1.045×10^{-3} a. u. (=0.02843 eV) in all of the calculations. The solutions of Eqs. 8 and 9 for the cases of $N = 1$ and $N = 3$ are shown in Tables 1, 2, and 3. In the exact numerical calculations performed using the Schrödinger equation (2) mentioned below, the adjacent energy levels are separated by equal intervals, E_{int}, as shown in Fig. 2b. Detailed investigation of the solutions of Eqs. 4–13 as a function of N is very important because it will turn out that the numerical results of the analytical expressions show the similar tendency as the more exact solutions of the Schrödinger equations (18–20), and it gives an insightful clue to the elucidation of those more exact solutions, as shown below. In addition, the analytical solutions of Eqs. 4–13 can be divided into several exponential factors that cannot be understood just by solving Eq. 2 numerically, which implies that we may obtain an oscillatory time dependence of physical quantities of interest. Furthermore, detailed examination of the behavior of the former solutions may give an important hint of how to maximize the difference between direct photo-injection and dye excitation in real dye-sensitized solar cells.

First, we concentrate on Fig. 3, where N was set to unity. For the following discussion, refer to the values shown in Table 1. The quantities $\left|d_g^{(1)}\exp(s_1t)\right|^2$, $\left|d_g^{(2)}\exp(s_2t)\right|^2$, and $\left|d_g^{(3)}\exp(s_3t)\right|^2$ are independent of time during the time interval $0\le t\le t_{\text{off}}$ because s_1, s_2, and s_3 are so small that s_1t, s_2t, and s_3t are also very small. Among these, the principal contribution to $\left|d_g(t)\right|^2$ stems from $\left|d_g^{(1)}\exp(s_1t)\right|^2$ because $\left|d_g^{(1)}\right|$ is the largest. The main contribution to the time variation of $\left|d_g(t)\right|^2$ comes from $2\text{Re}\left\{d_g^{(1)}\exp(s_1t)d_g^{(2)*}\exp\quad(-s_2t)\right\} = 2\text{Re}\left\{d_g^{(1)}\exp(s_1t)\right.$ $\left.d_g^{(3)*}\exp(-s_3t)\right\}$, which have a fairly large time-dependent factor because they are not squared. In fact, the black line in Fig. 3a follows the time evolution of $2\text{Re}\left\{d_g^{(1)}\exp(s_1t)d_g^{(2)*}\exp(-s_2t)\right\}$, which becomes negative. The populations $\left|d_e^{(1)}\exp(s_1t)\right|^2$, $\left|d_e^{(2)}\exp(s_2t)\right|^2$,

Table 1 Solutions of Eqs. 8 and 9 for the cases of $N = 1$, $\vec{E}_0 \cdot \vec{d}_{ge} = 1.0 \times 10^{-10}$ a. u., $\vec{E}_0 \cdot \vec{d}_{gi} = 1.0 \times 10^{-3}$ a. u., and $N = 1$, $\vec{E}_0 \cdot \vec{d}_{ge} = 1.0 \times 10^{-3}$ a. u., $\vec{E}_0 \cdot \vec{d}_{gi} = 1.0 \times 10^{-10}$ a. u

s_1/fs^{-1}	s_2/fs^{-1}	s_3/fs^{-1}	$\left\|d_g^{(1)}\right\|$	$\left\|d_g^{(2)}\right\|$	$\left\|d_g^{(3)}\right\|$	$\left\|d_e^{(1)}\right\|$	$\left\|d_e^{(2)}\right\|$	$\left\|d_e^{(3)}\right\|$	$\left\|d_i^{(1)}\right\|$	$\left\|d_i^{(2)}\right\|$	$\left\|d_i^{(3)}\right\|$
1.793×10^{-17} $+1.610 \times 10^{-9}i$	-1.121×10^{-17} $+4.789 \times 10^{-2}i$	-6.723×10^{-18} $-4.789 \times 10^{-2}i$	0.8137	0.09315	0.09315	0.3894	0.1947	0.1947	2.443×10^{-8}	0.2158	0.2158

Table 2 Solutions of Eqs. 8 and 9 for the case of $N = 3$, $\vec{E}_0 \cdot \vec{d}_{ge} = 1.0 \times 10^{-10}$ a. u., $\vec{E}_0 \cdot \vec{d}_{gi} = 1.0 \times 10^{-3}$ a. u.

s_1/fs^{-1}	s_2/fs^{-1}	s_3/fs^{-1}	$\left\|d_g^{(1)}\right\|$	$\left\|d_g^{(2)}\right\|$	$\left\|d_g^{(3)}\right\|$	$\left\|d_e^{(1)}\right\|$	$\left\|d_e^{(2)}\right\|$	$\left\|d_e^{(3)}\right\|$	$\left\|d_i^{(1)}\right\|$	$\left\|d_i^{(2)}\right\|$	$\left\|d_i^{(3)}\right\|$
7.172×10^{-17} $+1.610 \times 10^{-9}i$	-4.034×10^{-17} $+8.295 \times 10^{-2}i$	-3.138×10^{-17} $-8.295 \times 10^{-2}i$	0.8137	0.09315	0.09315	0.3894	0.1947	0.1947	8.143×10^{-9}	0.1246	0.1246

Table 3 Solutions of Eqs. 8 and 9 for the case of $N = 3$, $\vec{E}_0 \cdot \vec{d}_{ge} = 1.0 \times 10^{-3}$ a. u., $\vec{E}_0 \cdot \vec{d}_{gi} = 1.0 \times 10^{-10}$ a. u.

s_1/fs^{-1}	s_2/fs^{-1}	s_3/fs^{-1}	$\left\|d_g^{(1)}\right\|$	$\left\|d_g^{(2)}\right\|$	$\left\|d_g^{(3)}\right\|$	$\left\|d_e^{(1)}\right\|$	$\left\|d_e^{(2)}\right\|$	$\left\|d_e^{(3)}\right\|$	$\left\|d_i^{(1)}\right\|$	$\left\|d_i^{(2)}\right\|$	$\left\|d_i^{(3)}\right\|$
8.068×10^{-17} $+1.838 \times 10^{-9}i$	-4.482×10^{-17} $+7.762 \times 10^{-2}i$	-3.586×10^{-17} $-7.762 \times 10^{-2}i$	0.9291	0.03545	0.03545	3.815×10^{-8}	0.1331	0.1331	0.1482	7.410×10^{-2}	7.410×10^{-2}

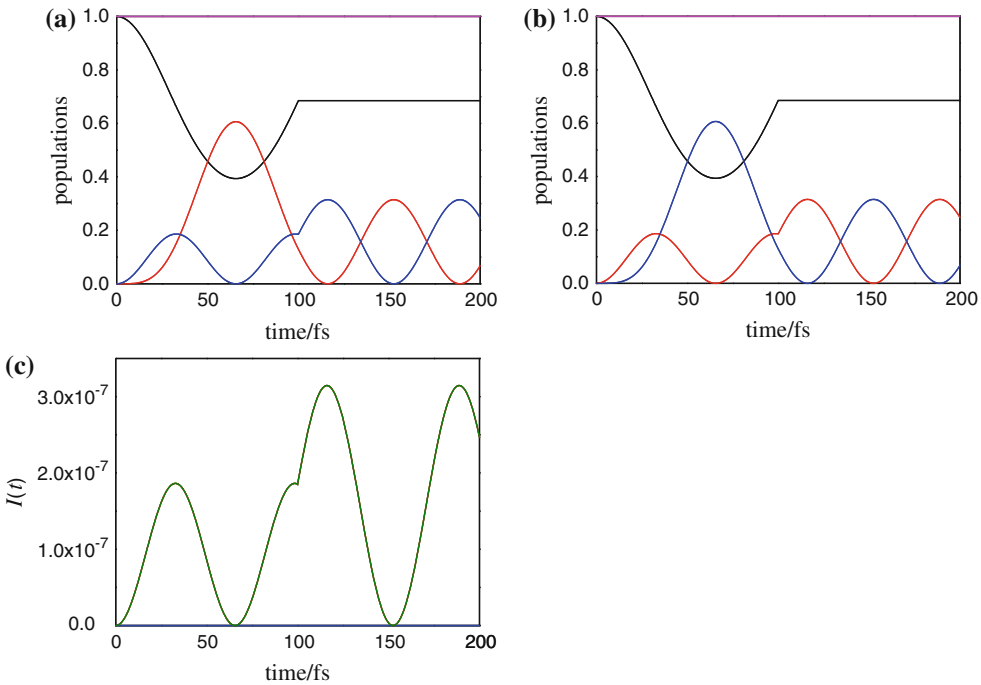

Fig. 3 Time evolution of populations and time-dependent fluorescence, $I(t)$, for the case of $N = 1$. **a** Populations for the case of $\vec{E}_0 \cdot \vec{d}_{ge} = 1.0 \times 10^{-10}$ a. u. and $\vec{E}_0 \cdot \vec{d}_{gi} = 1.0 \times 10^{-3}$ a. u. (direct photo-injection). **b** Populations for the case of $\vec{E}_0 \cdot \vec{d}_{ge} = 1.0 \times 10^{-3}$ a. u. and $\vec{E}_0 \cdot \vec{d}_{gi} = 1.0 \times 10^{-10}$ a. u. (dye excitation). **c** Time-dependent fluorescence, $I(t)$, for the cases of both (**a**) and (**b**). In **a** and **b**, the *black line* represents state g, the *red line* state e, and the *blue line* state i

$\left|d_e^{(3)} \exp(s_3 t)\right|^2$, $\left|d_i^{(1)} \exp(s_1 t)\right|^2$, $\left|d_i^{(2)} \exp(s_2 t)\right|^2$, and $\left|d_i^{(3)} \exp(s_3 t)\right|^2$ are also independent of time during the time interval $0 \leq t \leq t_{\text{off}}$ because s_1, s_2, and s_3 are quite small. The constant contributions to $|d_e(t)|^2$ and $|d_i(t)|^2$ stem from $\left|d_e^{(1)} \exp(s_1 t)\right|^2$, and $\left|d_i^{(2)} \exp(s_2 t)\right|^2$ and $\left|d_i^{(3)} \exp(s_3 t)\right|^2$, respectively, as can easily be understood from Table 1.

The time-dependent contribution to $|d_e(t)|^2$ is comparable in magnitude to $2\mathrm{Re}\left\{d_e^{(2)}\exp(s_2t)d_e^{(3)*}\exp(-s_3t)\right\}$ and $2\mathrm{Re}\left\{d_e^{(1)}\exp(s_1t)d_e^{(2)*}\exp(-s_2t)\right\} = 2\mathrm{Re}\left\{d_e^{(1)}\exp(s_1t)d_e^{(3)*}\exp(-s_3t)\right\}$. The time-dependent contribution to $|d_i(t)|^2$ is more dominant from $2\mathrm{Re}\left\{d_i^{(2)}\exp(s_2t)d_i^{(3)*}\exp(-s_3t)\right\}$ than from $2\mathrm{Re}\left\{d_i^{(1)}\exp(s_1t)d_i^{(2)*}\exp(-s_2t)\right\}$ and $2\mathrm{Re}\left\{d_i^{(1)}\exp(s_1t)d_i^{(3)*}\exp(-s_3t)\right\}$ because $\left|d_i^{(1)}\right|$ is very small as can be seen from Table 1. The time dependence of the black line in Fig. 3a is very similar to that of $2\mathrm{Re}\left\{d_i^{(2)}\exp(s_2t)d_i^{(3)*}\exp(-s_3t)\right\}$.

Next, we consider the time interval $t_{\mathrm{off}} \le t \le t_{\mathrm{final}}$. The population of state g, $|d_g(t)|^2$, is constant as can be understood from Eq. 10. This is clearly seen by the black line in Fig. 3a. This is simply because state g is disconnected from the other states if the laser pulse is off, as can be seen from the Schrödinger equation (2). The quantities $\left|d_4\exp\left\{i\sqrt{N}V(t-t_{\mathrm{off}})/\hbar\right\}\right|^2$ and $\left|d_5\exp\left\{-i\sqrt{N}V(t-t_{\mathrm{off}})/\hbar\right\}\right|^2$ are independent of time during the time interval because d_4 and d_5 are constants and the exponential terms have no influence on the time dependence. Therefore, the time dependence of $|d_e(t)|^2$ and $|d_i(t)|^2$ originates only from the terms $2\mathrm{Re}\left[d_4d_5^*\exp\left\{2i\sqrt{N}V(t-t_{\mathrm{off}})/\hbar\right\}\right]$ and $-2\mathrm{Re}\left[\frac{d_4d_5^*}{\sqrt{N}}\exp\left\{2i\sqrt{N}V(t-t_{\mathrm{off}})/\hbar\right\}\right]$, respectively. Because these two terms have opposite sign, $|d_e(t)|^2$ increases when $|d_i(t)|^2$ decreases and vice versa, as can be seen by red and blue lines in Fig. 3a.

In the special case of Fig. 3, we notice that the time evolutions of the cases (a) and (b) are reversed. This is reasonable because states e and i are on the same footing using any given parameters. Although the total time-dependent fluorescence, $I(t)$, is the same for both direct photo-injection and dye excitation, as shown in Fig. 3c, the contribution to it stems from different sources. The population of state i dominates $I(t)$ in the case of direct photo-injection, whereas the population of state e dominates $I(t)$ in the case of dye excitation because of the much larger transition dipole moments in either case. However, unfortunately, we cannot judge whether direct photo-injection or dye excitation takes place by investigating the time-dependent fluorescence in this case.

Next, we concentrate on Fig. 4 where N was set to be 3. In this case, E_{int} was set to be 2.9×10^{-4} eV. For the following discussion, refer to the values shown in Tables 2 and 3. As in Fig. 3, the quantities $\left|d_g^{(1)}\exp(s_1t)\right|^2$, $\left|d_g^{(2)}\exp(s_2t)\right|^2$, and $\left|d_g^{(3)}\exp(s_3t)\right|^2$ are independent of time during the time interval $0 \le t \le t_{\mathrm{off}}$ because s_1, s_2, and s_3 are again so small that s_1t, s_2t, and s_3t are also very small. Among these quantities, the main contribution to $|d_g(t)|^2$ stems from $\left|d_g^{(1)}\exp(s_1t)\right|^2$ because $\left|d_g^{(1)}\right|$ is the largest term, as in Fig. 3. The principal contribution to time variation of $|d_g(t)|^2$ comes from $2\mathrm{Re}\left\{d_g^{(1)}\exp(s_1t)d_g^{(2)*}\exp(-s_2t)\right\} = 2\mathrm{Re}\left\{d_g^{(1)}\exp(s_1t)d_g^{(3)*}\exp(-s_3t)\right\}$, which have a fairly large time-dependent factor because they also are not squared. Actually, the black lines in panels (a) and (b) almost follow the time evolution of $2\mathrm{Re}\left\{d_g^{(1)}\exp(s_1t)d_g^{(2)*}\exp(-s_2t)\right\}$, which sometimes becomes negative. Unlike Fig. 3, it is important to note that because $\left|d_g^{(1)}d_g^{(2)*}\right|$ is smaller for Fig. 4b than for Fig. 4a, the population decrease of state g is less significant for Fig. 4b than for Fig. 4a. The populations $\left|d_e^{(1)}\exp(s_1t)\right|^2$, $\left|d_e^{(2)}\exp(s_2t)\right|^2$, $\left|d_e^{(3)}\exp(s_3t)\right|^2$, $\left|d_i^{(1)}\exp(s_1t)\right|^2$, $\left|d_i^{(2)}\exp(s_2t)\right|^2$, and $\left|d_i^{(3)}\exp(s_3t)\right|^2$ are also independent of time during the time interval $0 \le t \le t_{\mathrm{off}}$ because s_1, s_2, and s_3 are quite small also. The constant contributions to $|d_e(t)|^2$ and $|d_i(t)|^2$ stem from $\left|d_e^{(1)}\exp(s_1t)\right|^2$, and $\left|d_i^{(2)}\exp(s_2t)\right|^2$ and $\left|d_i^{(3)}\exp(s_3t)\right|^2$, respectively, as can easily be understood from Tables 2 and 3. Because the quantities $\left|d_e^{(1)}\right|$, $\left|d_e^{(2)}\right|$, and $\left|d_e^{(3)}\right|$ are larger than the quantities $\left|d_i^{(1)}\right|$, $\left|d_i^{(2)}\right|$, and $\left|d_i^{(3)}\right|$ in Fig. 4a, the population of state e can become larger than that of state i. On the other hand, because the quantities $\left|d_e^{(1)}\right|$, $\left|d_e^{(2)}\right|$, and $\left|d_e^{(3)}\right|$ are not necessarily larger than the quantities $\left|d_i^{(1)}\right|$, $\left|d_i^{(2)}\right|$, and $\left|d_i^{(3)}\right|$ in Fig. 4b, the population of state e can become comparable to that of the state i. In the time-dependent contribution to $|d_e(t)|^2$, $2\mathrm{Re}\left\{d_e^{(1)}\exp(s_1t)d_e^{(2)*}\exp(-s_2t)\right\} = 2\mathrm{Re}\left\{d_e^{(1)}\exp(s_1t)d_e^{(3)*}\exp(-s_3t)\right\}$ and $2\mathrm{Re}\left\{d_e^{(2)}\exp(s_2t)d_e^{(3)*}\exp(-s_3t)\right\}$, because the former can become a little bit larger than the latter in Fig. 4a, the total population $|d_e(t)|^2$ reflects the behavior of $2\mathrm{Re}\left\{d_e^{(1)}\exp(s_1t)d_e^{(2)*}\exp(-s_2t)\right\}$. In particular, because both $2\mathrm{Re}\left\{d_e^{(1)}\exp(s_1t)d_e^{(2)*}\exp(-s_2t)\right\}$ and $2\mathrm{Re}\left\{d_e^{(2)}\exp(s_2t)d_e^{(3)*}\exp(-s_3t)\right\}$ become largest at around 40 fs, we can see a large peak for the red line at this time in Fig. 4a. However, in Fig. 4b, because

$2\mathrm{Re}\left\{d_e^{(2)}\exp(s_2t)d_e^{(3)*}\exp(-s_3t)\right\}$ can become much larger than $2\mathrm{Re}\left\{d_e^{(1)}\exp(s_1t)d_e^{(2)*}\exp(-s_2t)\right\} = 2\mathrm{Re}\left\{d_e^{(1)}\exp(s_1t)d_e^{(3)*}\exp(-s_3t)\right\}$, the total population $|d_e(t)|^2$ reflects the behavior of $2\mathrm{Re}\left\{d_e^{(2)}\exp(s_2t)d_e^{(3)*}\exp(-s_3t)\right\}$, which frequently oscillates. On the other hand, in the time-dependent contribution to $|d_i(t)|^2$, $2\mathrm{Re}\left\{d_e^{(1)}\exp(s_1t)d_e^{(2)*}\exp(-s_2t)\right\} = 2\mathrm{Re}\left\{d_e^{(1)}\exp(s_1t)d_e^{(3)*}\exp(-s_3t)\right\}$ and $2\mathrm{Re}\left\{d_e^{(2)}\exp(s_2t)\,d_e^{(3)*}\exp(-s_3t)\right\}$, because the former can become much smaller than the latter in Fig. 4a, the total population $|d_i(t)|^2$ reflects the behavior of $2\mathrm{Re}\left\{d_i^{(2)}\exp(s_2t)d_i^{(3)*}\exp(-s_3t)\right\}$. However, in Fig. 4b, because $2\mathrm{Re}\left\{d_i^{(1)}\exp(s_1t)d_i^{(2)*}\exp(-s_2t)\right\} = 2\mathrm{Re}\left\{d_i^{(1)}\exp(s_1t)d_i^{(3)*}\exp(-s_3t)\right\}$ can become a little bit larger than $2\mathrm{Re}\left\{d_i^{(2)}\exp(s_2t)d_i^{(3)*}\exp(-s_3t)\right\}$, the total population $|d_i(t)|^2$ reflects the behavior of $2\mathrm{Re}\left\{d_i^{(1)}\exp(s_1t)d_i^{(2)*}\exp(-s_2t)\right\}$, which oscillates about once. In particular, because both $2\mathrm{Re}\left\{d_i^{(2)}\exp(s_2t)d_i^{(3)*}\exp(-s_3t)\right\}$ and $2\mathrm{Re}\left\{d_i^{(1)}\exp(s_1t)d_i^{(2)*}\exp(-s_2t)\right\}$ become largest at around 40 fs, we can see a large peak of the blue line at this time in Fig. 4b.

As can easily be understood from Eqs. 10–13, when N becomes larger, the oscillations of populations and time-dependent fluorescence become more frequent for the time interval $t_{\mathrm{off}} \leq t \leq t_{\mathrm{final}}$. This can be concretely confirmed by comparing Figs. 4 with 3. It should also be noted that the symmetry between dye excitation and direct photo-injection observed in Fig. 3 is now broken. Because of the presence of more states involved in excitation in direct photo-injection, there remain higher populations in states e and i for direct photo-injection (Fig. 4a) than for dye excitation (Fig. 4b) after irradiation by the laser pulse.

Unlike the total time-dependent fluorescence, $I(t)$, shown in Fig. 3c, it is fairly different for direct photo-injection and dye excitation, as shown in panels (c) and (d), respectively. The population of state i and the coherence dominate $I(t)$ in the case of direct photo-injection, whereas the population of state e dominates $I(t)$ in the case of dye excitation because of the much larger transition dipole moments in either case. Also note that the magnitude of $I(t)$ is different for the two cases. Therefore, one may expect to be able to expect to judge whether direct photo-

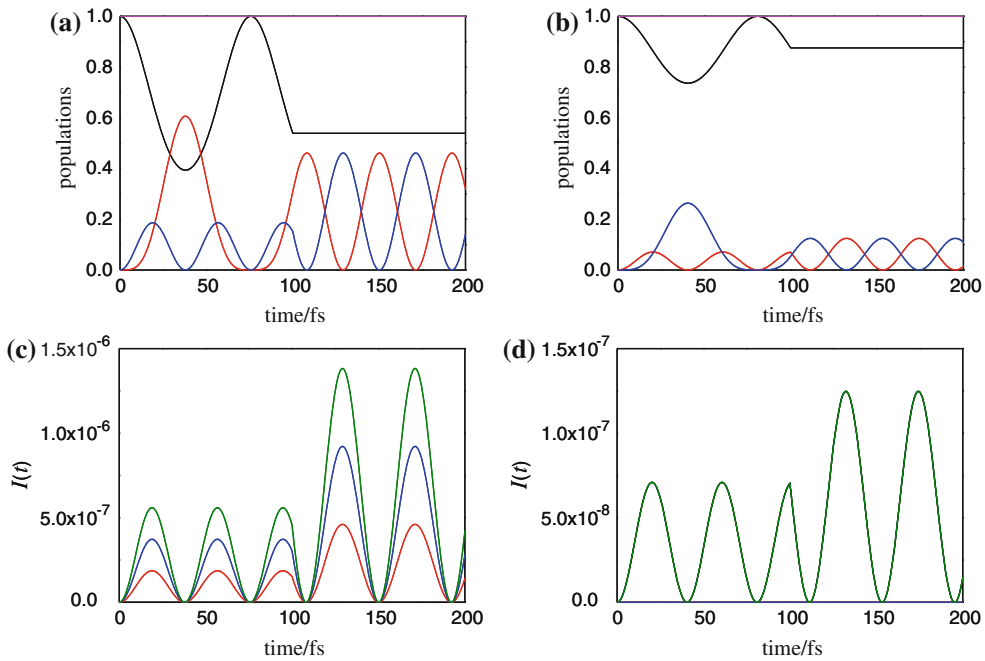

Fig. 4 Time evolution of populations and time-dependent fluorescence, $I(t)$, for the case of $N = 3$. **a** Populations for the case of $\vec{E}_0 \cdot \vec{d}_{ge} = 1.0 \times 10^{-10}$ a. u. and $\vec{E}_0 \cdot \vec{d}_{gi} = 1.0 \times 10^{-3}$ a. u. (direct photo-injection). **b** Populations for the case of $\vec{E}_0 \cdot \vec{d}_{ge} = 1.0 \times 10^{-3}$ a. u. and $\vec{E}_0 \cdot \vec{d}_{gi} = 1.0 \times 10^{-10}$ a. u. (dye excitation). **c** Time-dependent fluorescence, $I(t)$, for the case of **a**. **d** Time-dependent fluorescence, $I(t)$, for the case of (**b**). In **a** and **b**, the *black line* represents state g, the *red line* state e, and the *blue line* state i. In **c** and **d**, the contribution from the population of state e is shown by the *black line*, that from the population of state i is shown by the *red line*, that from the coherence terms is shown by the *blue line*, and the total time-dependent fluorescence, $I(t)$, is shown by the *green line*. Note that in **d**, the *black line* is superimposed by the *green line*

injection or dye excitation takes place by inspecting the time-dependent fluorescence if N becomes larger (i.e., the continuum of the conduction band of the semiconductor is taken into account).

The agreement with exact calculations is excellent in all of the analytical calculation results shown above. This implies that the analytical expressions derived above, only assuming the rotating-wave approximation, provide useful insight into the elucidation of the difference between direct photo-injection and dye excitation. Therefore, in our opinion, the simple laser-driven system that mimics electron-injection dynamics in dye-sensitized solar cells is worthy of detailed study.

From the calculation results where N is more than 500 and $E_{\rm int}$ was set to be 2.9×10^{-4} eV, it was found that the exact numerical results and the analytical results agree very well for dye excitation, but they do not agree for direct photo-injection at all. This may be because when N becomes larger, the laser couplings between state g and states $i_{\rm j}$ become quite different from those in the case of the analytical expressions, where it is assumed that $E_e - E_g = E_{i_1} - E_g = E_{i_2} - E_g = \cdots = E_{i_N} - E_g = \hbar\omega$. However, in the former case, because there is only one laser coupling between state g and state e, the discrepancy was negligibly small. Therefore, because there is no meaning in comparing the case of direct photo-injection and that of dye excitation, we do not show these results in the present paper.

The more realistic situation that was estimated by solving Eqs. 18–20 is shown in Fig. 5. In this case, the incident laser pulse is assumed to have the form

$$\vec{E}(t) = \vec{E}_0 \sin^2(\pi t/t_{\rm off}) \cos(\omega t) \quad \text{for } 0 \le t \le t_{\rm off}, \tag{34}$$

$$\vec{E}(t) = 0 \quad \text{for } t_{\rm off} \le t \le t_{\rm final}. \tag{35}$$

This type of laser pulse has slow turn-on and turn-off so that it mimics experimentally realizable laser-pulse shape very well. In addition, this model takes into account the vibrational degrees of freedom of the attached molecule and relaxation of the injected electron in the conduction band of the semiconductor. In fact, the parameters in the Schrödinger equation (18–20), E_g, E_e, E_c, $\hbar\omega_{\rm vib}$, $\bar{V}$, $\bar{\mathcal{N}}$, $\hbar\omega_{\rm max}$ were set to be 0.0, 2.952, 1.0, 0.1, 0.1, 1, 2.2 eV, respectively. Because these values correspond to the typical values to the TiO_2-cathecol system, the calculation results shown below are the more realistic descriptions of dye-sensitized solar cells.

From Fig. 5, we can see that the dye excitation shows no significant quantum beat (Fig. 5b), while the direct photo-injection shows a significant quantum beat (Fig. 5a). Note also that the intensity of the time-dependent fluorescence differs between direct photo-injection and dye excitation by several orders of magnitude. This difference has already been seen in Fig. 4, where only three continuum states were considered (compare panels (c) and (d) in Fig. 4). This is because infinitely many continuum states are excited via direct photo-injection by lasers. Further, we notice that the time-dependent fluorescence decays with time, which agrees with the reported experimental and theoretical results [37, 39–41]. More importantly, as in Fig. 4, the population of state i and the coherence dominate $I(t)$ in the case of direct photo-injection (Fig. 5a), whereas the population of state e dominates $I(t)$ in the case of dye excitation (Fig. 5b) because of the much larger transition dipole moments in either case. Note that in Fig. 5b, the black line and the green line are superimposed. This has already been pointed out in the explanation of Fig. 4 above. Therefore, again, the simple analytical expressions derived in Sect. 2 have been very illuminating for clarifying the difference

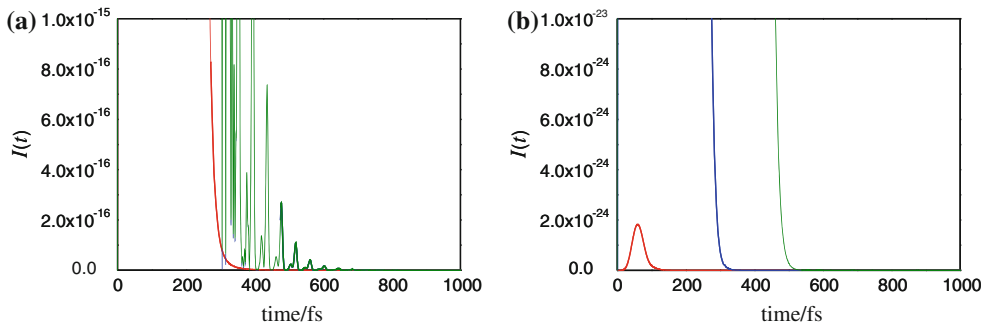

Fig. 5 Time-dependent fluorescence, $I(t)$, calculated by solving Eqs. 18–20 and Eq. 30. Panel **a** is for the case of $\vec{E}_0 \cdot \vec{d}_{ge} = 1.0 \times 10^{-10}$ a. u. and $\vec{E}_0 \cdot \vec{d}_{gi} = 1.0 \times 10^{-3}$ a. u. (direct photo-injection), and panel **b** is for the case of $\vec{E}_0 \cdot \vec{d}_{ge} = 1.0 \times 10^{-3}$ a. u. and $\vec{E}_0 \cdot \vec{d}_{gi} = 1.0 \times 10^{-10}$ a. u. (dye excitation). In **a** and **b**, the contribution from the population of state e is shown by the *black line*, that from the population of state i is shown by the *red line*, that from the coherence terms is shown by the *blue line*, and the total time-dependent fluorescence, $I(t)$, is shown by the *green line*. Because the intensity of the time-dependent fluorescence between $t = 0$ and $t = 500$ fs is too strong to explore the quantum beat, the intensity during this period is not shown in the figure

between direct photo-injection and dye excitation in the present more realistic calculations.

The last example of Fig. 5 clearly indicates that one can discriminate dye excitation and direct photo-injection using the laser pulse and measurement of the time-dependent fluorescence: the fingerprint, quantum beat, is left on the time-dependent fluorescence in the case of direct photo-injection.

4 Conclusion

In this paper, we have theoretically and numerically investigated a new type of analytically solvable laser-driven system inspired by electron-injection dynamics in dye-sensitized solar cells. The simple analytical expressions were found to be quite illuminating for clarifying the difference between dye excitation and direct photo-injection occurring between dye molecules and semiconductor nanoparticles. More importantly, we have proposed a method for experimentally discriminating dye excitation and direct photo-injection using time-dependent fluorescence. We have found that dye excitation shows no significant quantum beat, whereas direct photo-injection shows a significant quantum beat by utilizing both the simple analytical expressions and more realistic models. The physical background for this difference was consistently explained using the simple analytical expressions. In fact, this implies that the calculations of Figs. 3 and 4 were worthy of detailed discussion.

It should also be noted that dye excitation and direct photo-injection can be controlled by adjusting the polarization direction of the incident light with respect to the transition dipole moment of the dye molecule, as can be seen from Eqs. 14–16.

Finally, May et al. have theoretically shown that the injection pathways can be discriminated by the time-independent linear absorption spectra [42]. Our method can be regarded as an alternative way for the discrimination in such a way as that Raman and IR spectra are complementary to each other for the identification of substances.

Acknowledgments This work was supported by Funding Program for World-Leading Innovative R&D on Science and Technology (FIRST) "Development of Organic Photovoltaics toward a Low-Carbon Society," Cabinet Office, Japan. The authors wish to thank Dr. J. Fujisawa and Dr. M. Nagata for useful comments and discussions.

References

1. Allen L, Eberly JH (1975) Optical resonance and two-level atoms. Wiley, New York
2. Cohen-Tannoudji C, Dupont-Roc J, Grynberg G (1992) Atom-photon interactions. Wiley, New York
3. Louisell WH (1973) Quantum statistical properties of radiation. Wiley, New York
4. Loudon R (2000) The quantum theory of light. Oxford University Press, New York
5. Demtröder W (2009) Laser spectroscopy. Springer, Berlin
6. Rice SA, Zhao N (2000) Optical control of molecular dynamics. Wiley, New York
7. Shapiro M, Brumer P (2003) Principles of the quantum control of molecular processes. Wiley, New York
8. Shore BW, Ackerhalt J (1977) Phys Rev A 15:1640
9. Bowden CM, Sung CC (1979) Phys Rev A 20:2033
10. Tsukada N, Tsujinishi R, Nagano M, Tomishima K (1980) Phys Rev A 21:1281
11. Kyrölä E, Salomaa R (1981) Phys Rev A 23:1874
12. Hioe FT (1983) Phys Rev A 28:879
13. Carroll CE, Hioe FT (1987) Phys Rev A 36:724
14. Carroll CE, Hioe FT (1988) J Math Phys 29:487
15. Djotyan GP, Bakos JS, Sörlei Z (2001) Phys Rev A 64:013408
16. Rabin Y, Ben-Reuven A (1979) Phys Rev A 19:1697
17. Cook RJ, Shore BW (1979) Phys Rev A 20:539
18. Hougen JT (1976) J Chem Phys 65:1035
19. Stone J, Goodman MF, Dows DA (1976) J Chem Phys 65:5062
20. Goodman MF, Stone J, Dows DA (1976) J Chem Phys 65:5052
21. Narducci LM, Mitra SS, Shatas RA, Coulter CA (1977) Phys Rev A 16:247
22. Shore BW (1981) Phys Rev A 24:1413
23. Levine AM, Schreiber WM, Weiszmann AN (1982) Phys Rev A 25:625
24. Bergmann K, Theuer H, Shore BW (1998) Rev Mod Phys 70:1003
25. O' Regan B, Grätzel M (1991) Nature 353:737
26. Kroon JM, Bakker NJ, Smit HJP, Liska P, Thampi KR, Wang P, Zakeeruddin SM, Grätzel M, Hinsch A, Hore S, Würfel U, Sastrawan R, Durrant JR, Palomares E, Pettersson H, Gruszecki T, Walter J, Skupien K, Tulloch GE (2007) Prog Photovolt Res Appl 15:1
27. Duncan WR, Prezhdo OV (2007) Annu Rev Phys Chem 58:143
28. Persson P, Bergström R, Lunell S (2000) J Phys Chem B 104:10348
29. Xu Y, Chen W, Liu S, Cao M, Li J (2007) Chem Phys 331:275
30. Redfern PC, Zapol P, Curtiss LA, Rajh T, Thurnauer MC (2003) J Phys Chem B 107:11419
31. Moser J, Punchihewa S, Infelta PP, Grätzel M (1991) Langmuir 7:3012
32. Rodriguez R, Blesa MA, Regazzoni AE (1996) J Colloid Interface Sci 177:122
33. Liu Y, Dadap JI, Zimdars D, Eisenthal KB (1999) J Phys Chem B 103:2480
34. Watson DF, Meyer GJ (2005) Annu Rev Phys Chem 56:119
35. Kubo T, Fujisawa J, Segawa H (2009) Electrochem 77:977
36. Rego LGC, Batista VS (2003) J Am Chem Soc 125:7989
37. Wang L, May V (2004) J Chem Phys 121:8039
38. Kono H, Fujimura Y, Lin SH (1981) J Chem Phys 75:2569
39. Hannappel T, Burfeindt B, Storck W, Willig F (1997) J Phys Chem B 101:6799
40. Ramakrishna S, Willig F, May V, Knorr A (2003) J Phys Chem B 107:607
41. Zimmermann C, Willig F, Ramakrishna S, Burfeindt B, Pettinger B, Eichberger R, Storck W (2001) J Phys Chem B 105:9245
42. Wang L, Willig F, May V (2007) J Chem Phys 126:134110